●●●

Energy input from quasars regulates the growth and activity of black holes and their host galaxies

Tiziana Di Matteo[1]*, **Volker Springel**[1] & **Lars Hernquist**[2]

[1]*Max-Planck-Institut für Astrophysik, Karl-Schwarzschild-Strasse 1, 85740 Garching bei München, Germany*
[2]*Astronomy Department, Harvard University, 60 Garden Street, Cambridge, Massachusetts 02138, USA*

* Present address: Department of Physics, Carnegie-Mellon University, 5000 Forbes Avenue, Pittsburgh, Pennsylvania 15213, USA

....

In the early Universe, while galaxies were still forming, black holes as massive as a billion solar masses powered quasars. Supermassive black holes are found at the centres of most galaxies today[1–3], where their masses are related to the velocity dispersions of stars in their host galaxies and hence to the mass of the central bulge of the galaxy[4,5]. This suggests a link between the growth of the black holes and their host galaxies[6–9], which has indeed been assumed for a number of years. But the origin of the observed relation between black hole mass and stellar velocity dispersion, and its connection with the evolution of galaxies,

have remained unclear. Here we report simulations that simultaneously follow star formation and the growth of black holes during galaxy–galaxy collisions. We find that, in addition to generating a burst of star formation[10], a merger leads to strong inflows that feed gas to the supermassive black hole and thereby power the quasar. The energy released by the quasar expels enough gas to quench both star formation and further black hole growth. This determines the lifetime of the quasar phase (approaching 100 million years) and explains the relationship between the black hole mass and the stellar velocity dispersion.

A large fraction of the black hole mass in galaxies today is thought to have been assembled during the peak of quasar activity in the early Universe[11,12], when large amounts of matter were available for accretion onto central black holes. Interactions and mergers between galaxies are known to trigger large-scale nuclear gas inflows[13,14], which are required for the growth of central black holes by accretion. Also, hierarchical models of galaxy formation imply that mergers of galaxies form elliptical or spheroidal components in galaxies, by destroying stellar disks and triggering nuclear starbursts.

This has led to suggestions that the M_{BH}–σ relation (where M_{BH} is the black hole mass, and σ is the velocity dispersion of stars in the bulge of galaxies) could arise in galaxy mergers, provided that strong outflows are produced in response to major phases of accretion, capable of halting further black hole growth[8,15–17]. Indeed,
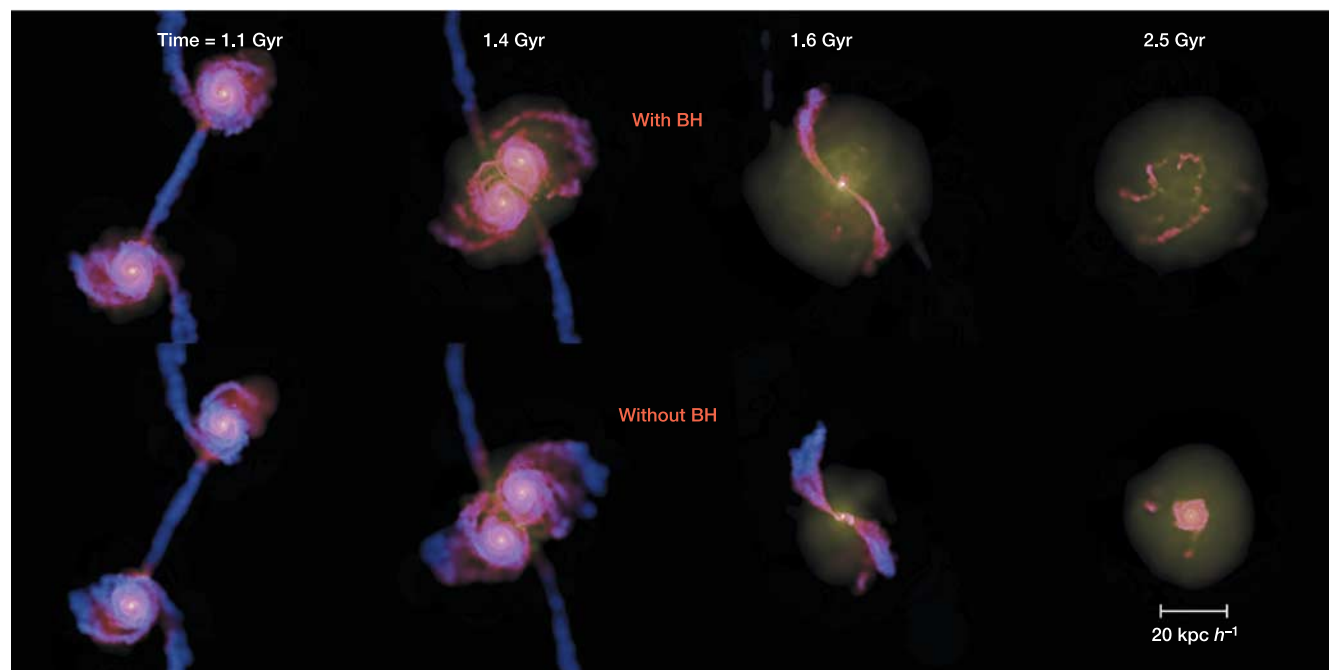

Figure 1 Snapshots of the simulated time evolution of mergers of two galaxies with and without black holes. The full time sequence for this simulation can be viewed in the Supplementary Video. Top and bottom panels show respectively the models with and without the inclusion of black holes (BH). In both cases, four snapshots at different times in the simulations are shown. The images visualize the projected gas distribution in the two galaxies, colour-coded by temperature (blue to red). The colliding galaxies have the same initial mass corresponding to a 'virial velocity' $V_{vir} = (M_{tot} \times 10GH_0)^{1/3} = 160\,\mathrm{km\,s^{-1}}$, and consist of an extended dark matter halo, a stellar bulge, and a disk made up of stars and 20% gas (here M_{tot} is the total halo mass, G is the gravitational constant and $H_0 = 100\,h\,\mathrm{km\,s^{-1}\,Mpc^{-1}}$ is the Hubble constant where we take the constant $h = 0.7$). Each individual galaxy in the simulations is represented with 30,000 particles for the dark matter, 20,000 for the stellar disk, 20,000 for the gaseous disk, and 10,000 for the bulge component. Two such galaxies were set up on a parabolic, prograde collision course, and then evolved forward in time numerically with GADGET-2 (ref. 29), a parallel tree-smooth-

particle-hydrodynamic simulation code. The first snapshot ($t = 1.1$ Gyr) shows the systems after the first passage of the two galaxies. The second snapshot (t = 1.4 Gyr) depicts the galaxies distorted by their mutual tidal interaction, just before they merge. The peak in the star formation and black hole accretion (see also Fig. 2) is reached at the time of the third snapshot ($t = 1.6$ Gyr), when the galaxies finally coalesce. At this time, a strong wind driven by feedback energy from the accretion expels much of the gas from the inner regions in the simulation with black holes. Finally, the last snapshot shows the systems after the galaxies have merged ($t = 2.5$ Gyr), leaving behind quasi-static spheroidal galaxies. In the simulation with black holes (top), the remnant is very gas poor and has little gas left that is dense enough to support ongoing star formation. This highlights the fact that the presence of supermassive black holes, which accrete matter from the surrounding gas and heat it with the associated feedback energy, dramatically alters the merger remnant. The scale bar shows the dimension in units of kpc h^{-1} (1 pc = 3.26 light years).

observations point to the existence of strong outflows in bright quasars[18–20]. In this picture, black hole accretion is expected to have a crucial effect on the evolution of the host galaxy. However, the coupling of star formation with black hole growth in the context of galaxy evolution is difficult to treat on the basis of analytical estimates alone.

We have, therefore, performed detailed numerical simulations of galaxy mergers that include radiative cooling, star formation, black hole growth, energetic feedback from supernovae and accretion onto black holes, as well as the gravitational dynamics of gas, stars and dark matter (see Supplementary Information and further details in ref. 21). As described in the Supplementary Information, we include a novel treatment of gas accretion onto supermassive black holes and its associated feedback in the centres of merging galaxies. We describe black holes using collisionless 'sink' particles that can grow in mass by accreting gas from their surroundings. The accretion rate is estimated by relating the small-scale, unresolved flow around the black hole to the large-scale, resolved gas properties using a spherical Bondi–Hoyle[22] model. We further assume that a small fraction, f, of the radiated luminosity couples thermodynamically to the surrounding gas. This 'feedback energy' gives an effective feedback energy heating rate $\dot{E}_{feed} = fL = f\eta\dot{M}c^2$, where we fix the radiative efficiency, η, to 0.1, the typical value derived from Shakura–Sunyaev[23] accretion models onto a non-rotating black hole. (Here c is the velocity of light, $L = \eta\dot{M}c^2$ is the accretion luminosity, and $\dot{M}$ is the mass accretion rate). We further assume that $f = 0.05$, so that ~0.5% of the accreted rest mass energy is available to heat the gas.

To illustrate the effect of central, supermassive black holes on mergers of two disk galaxies, we compare the gas evolution between two simulations involving galaxies that are roughly the size of the Milky Way (Fig. 1). Star formation and supernova feedback are included in both simulations, but we add our black hole growth and feedback model in one (top four panels of Fig. 1; see also Supplementary Video) and neglect it in the other (bottom four panels). The first pair of images (at time $t = 1.1$ Gyr) shows the galaxies soon after their first encounter, when strong gravitational forces have spawned extended tidal tails. At this time, the black holes in the centres of each galaxy (top panel) have already grown significantly from their initial masses and are accreting at a moderate level. However, the overall star formation rate is essentially unaffected by the presence of the black holes, as indicated by Fig. 2, which plots the star formation rate (in both cases), the black hole accretion rate and black hole mass (for the top panels of Fig. 1) as a function of time.

The second snapshot ($t = 1.4$ Gyr) in Fig. 1 shows the galaxies when they begin to coalesce. Here, the tidal interaction has distorted the disks into a pair of bisymmetric spirals, and gas is shocked between the two galaxies. The tidal response drives gas into the central regions of each galaxy. Although only weak starbursts and accretion events are triggered at this time, it is already evident that black hole feedback alters the thermodynamic state of the gas, as indicated by the relatively lower density and higher temperature of the gas surrounding the galaxies in the simulation with black holes. In fact, a significant wind has started to flow out of the centres.

When the galaxies finally merge, as shown in the third pair of images in Fig. 1 ($t = 1.6$ Gyr), much of the gas is quickly converted into stars in intense bursts of star formation[10]. Owing to the enhanced gas density, the black holes, which also merge to form one object, experience a rapid phase of accretion close to the Eddington rate, resulting in significant mass growth. Also, the morphologies of the remnants in the two simulations begin to differ significantly. In the model without black holes, most of the gas is still inflowing in a comparatively cool phase. In contrast, the simulations with black holes exhibit a significant change in thermodynamic state of the circumnuclear gas, which is heated by the feedback energy provided by the accretion and partly expelled in a powerful wind. During this strong accretion phase and for this

interval of time, the object would be a bright quasar with a specific lifetime.

Differences persist as the remnants settle into a relaxed state (fourth pair of images in Fig. 1, $t = 2.5$ Gyr). The remnant without black holes (bottom image) retains a large amount of dense cold gas, yielding prolonged star formation at a steady rate. However, in the simulation with supermassive black holes (top image), nearly all the gas is expelled from the centre, quenching star formation and black hole accretion itself. Consequently, the black hole mass saturates, quasar activity stops, and star formation is inhibited, so that the remnant resembles a 'dead' elliptical galaxy whose stellar population quickly reddens[24]. In the particular example we show, the remnant of this major merger is an elliptical galaxy. In the hierarchical model of galaxy formation, a new disk can grow around this spheroid, turning it into the bulge component of a spiral galaxy. In very gas-rich mergers, a disk component may even survive directly[25] (an example of this is shown in the Supplementary Figure). We therefore expect black holes in bulges of spiral galaxies to be assembled in a manner similar to those in ellipticals. Our results should also apply for cases involving minor mergers.

The evolution of star formation rate, black hole accretion rate and black hole mass for mergers when the progenitor galaxy mass is varied (including the model shown in Fig. 1) are shown in Fig. 2. Models with different mass qualitatively reproduce the key features of the evolution shown in Fig. 1: the star formation and black hole accretion rates are both quenched in the remnant, and black hole growth saturates owing to feedback provided by accretion energy. However, the damping of star formation and black hole activity is
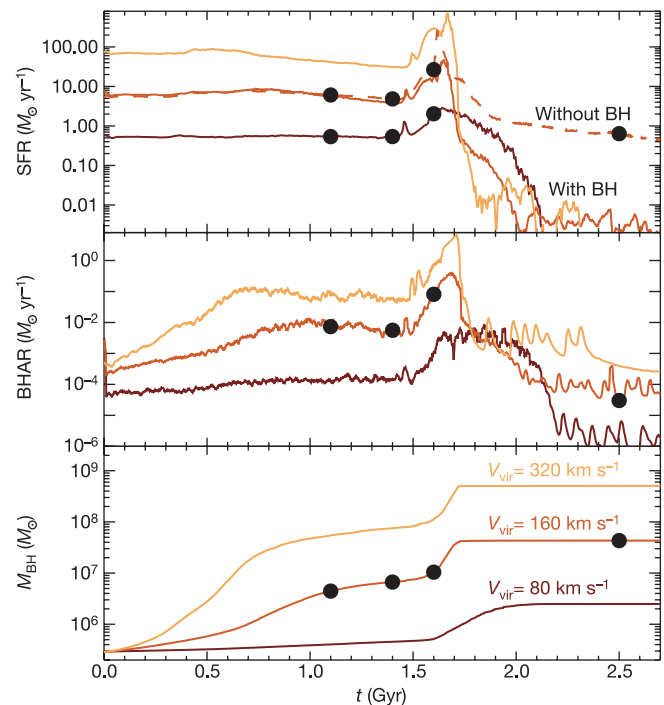

Figure 2 Black hole activity, star formation and black hole growth plotted as a function of time during a galaxy–galaxy merger. The star formation rate (SFR), black hole accretion rate (BHAR) and black hole mass are shown in the top, middle and bottom panels, respectively. The three lines in each panel (black, red and orange) correspond to models with galaxies of virial velocity $V_{vir} = 80$, 160 and 320 km s^{-1}, respectively. For comparison, we also show (top panel, dashed line) the evolution of the star formation rate for the model without a black hole that is shown in Fig. 1 (for the $V_{vir} = 160$ km s^{-1} galaxy). We note, in particular, that owing to AGN feedback, the peak amplitude of the starburst during the merger is lowered by a significant factor. The black filled circles in the individual panels identify the times of the corresponding snapshots shown in Fig. 1.

more abrupt in the more massive systems. Here, the total gas supply for accretion is larger, and the gravitational potential well is deeper, and so the black hole has to grow much more before its released energy is sufficient to expel the gas in a quasar driven wind, which then terminates further nuclear accretion and star formation. For the same reasons, the initial growth of the black holes, which is regulated by the properties of nearby gas, depends on the total mass. It is faster in more massive systems, which can therefore reach the exponential, Eddington-limited growth phase more easily. The lifetime of the active black hole phase, however, increases for smaller black hole masses, implying that low-luminosity quasars should be more numerous than bright ones. This is consistent with them residing in a greater number of smaller galaxies and with what has been found in recent surveys[26,27].

The dependence of black hole growth on galaxy mass yields a relation between the stellar spheroid of the remnant galaxy and its central black hole. Figure 3 shows the black hole mass versus the stellar velocity dispersion of the merger remnants from our simulations, compared with observations. We show simulations with six different galaxy masses, each of which has been run with three different initial gas mass fractions of the galaxies' disks. Remarkably,
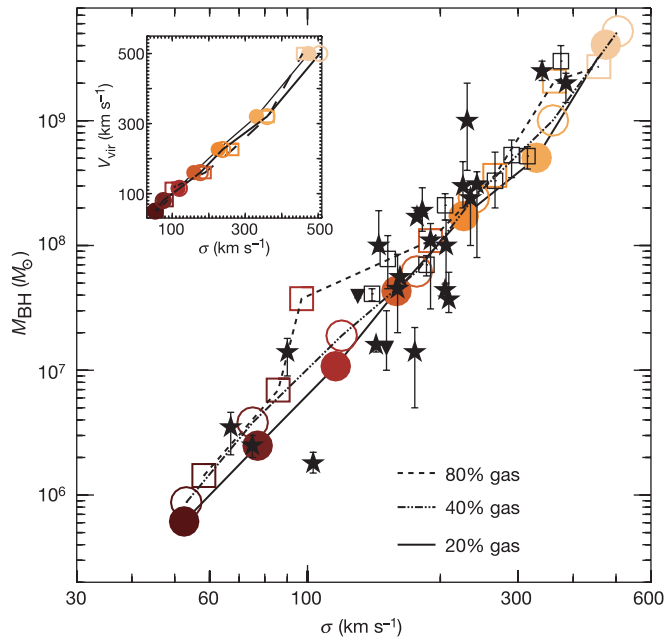
our simulations reproduce the observed M_{BH}–σ correlation very well. Note that black holes in more gas-rich mergers reach somewhat larger masses than those growing in gas-poorer environments (which is expected from our prescription for the accretion rate), but this is partly compensated by an increase in the velocity dispersion of the corresponding bulges, maintaining a comparatively tight M_{BH}–σ relation. However, this suggests that part of the intrinsic scatter in the observed relation can be ascribed to different gas fractions of the galaxies during black hole growth. Our lowest mass galaxy models probe a region of the M_{BH}–σ relation where few measurements are available, and predict that this correlation should hold towards small black hole masses and small velocity dispersions, in tentative agreement with recent observations[28].

Black hole growth is self-regulated in our models. As galaxies merge to form spheroids, the dynamical response of the gas to the energy supplied by accretion halts further growth once the black holes have reached a critical size for the gravitational potential of the bulge. At this saturation point, the active galactic nuclei (AGN) generate outflows that drive away gas and inhibit further star formation. Our simulations are, to our knowledge, the first self-consistent models to demonstrate that self-regulation can quantitatively account for the principle observational facts known for the local population of supermassive black holes, most notably the M_{BH}–σ relation. Moreover, self-regulation in our hydrodynamical simulations predicts a specific duration of the luminous episode of a black hole in a given galaxy, thereby explaining the origin of quasar lifetimes. We note that the final black hole masses we obtain are roughly proportional to the inverse of the value assumed for the feedback efficiency, f. We note that our choice of $f = 0.05$ is consistent with the value required in semi-analytic models[8] to explain the evolution of the number density of quasars.

The black hole accretion activity also has a profound effect on the host galaxy. The remnant spheroid is gas-poor and has low residual star formation, so it evolves to a red stellar colour on a short timescale. The simulations shown here make it possible to draw firm conclusions about this and other links between black hole growth, quasar activity and properties of the galaxy population. Our approach can also be implemented in cosmological simulations of hierarchical structure formation in representative pieces of the Universe. Such simulations will allow us to study directly why quasars were much more numerous in the early Universe than they are today, and how black holes and galaxies have influenced each other throughout cosmic history. □

Figure 3 The relation between the final black hole mass, M_{BH}, and the velocity dispersion of stars, σ, of our galaxy merger simulations compared with observational measurements. Filled circles show the masses of the black holes and the bulge velocity dispersions measured for the final remnants of six merger simulations of galaxies with disk gas fraction of 20%, but different total mass, parameterized by virial velocities of $V_{vir} = 50$, 80, 160, 320 and 500 km s^{-1} (shown by the dark to light red, from low- to high-mass galaxies respectively). Open circles and open squares with the same colour give results for gas fractions of 40% and 80%, respectively. We have also checked that our results are insensitive to the orbits of the galaxy collisions. Mimicking the observational data, we calculate σ as the line-of-sight stellar velocity dispersion of stars in the bulge within the effective radius, R_e, of the galaxy. Black symbols show observational data for the masses of supermassive black holes and the velocity dispersions of their host bulges; measurements based on stellar kinematics are denoted by black filled stars, those on gas kinematics by black open squares, and those on maser kinematics by black filled triangles. Details for all the displayed measurements and associated r.m.s. error bars are given in refs 3 and 27. The observed BH sample has been fitted by a power law relation, yielding[30]: $M_{BH} = (1.5 \pm 0.2) \times 10^8 \, M_\odot (\sigma/200)^{4.02 \pm 0.32}$ (here σ is in units of km s^{-1}). The inset shows the relation between the virial velocity, V_{vir}, and σ—shown in the x axis of the main panel—measured for the merger remnants in the simulations. The same colour coding is used as in the main panel to indicate corresponding mass objects.

1. Kormendy, J. & Richstone, D. Inward bound—The search for supermassive black holes in galactic nuclei. *Annu. Rev. Astron. Astrophys.* **33**, 581–624 (1995).
2. Magorrian, J. *et al.* The demography of massive dark objects in galaxy centers. *Astron. J.* **115**, 2285–2305 (1998).
3. Ferrarese, L. & Ford, H. C. Supermassive black holes in galactic nuclei: Past, present and future research. *Space Sci. Rev.* (in the press).
4. Ferrarese, L. & Merritt, D. A Fundamental relation between supermassive black holes and their host galaxies. *Astrophys. J.* **539**, L1–L4 (2000).
5. Gebhardt, K. *et al.* A relationship between nuclear black hole mass and galaxy velocity dispersion. *Astrophys. J.* **539**, L13–L16 (2000).
6. Kauffmann, G. & Haehnelt, M. A unified model for the evolution of galaxies and quasars. *Mon. Not. R. Astron. Soc.* **311**, 576–588 (2000).
7. Volonteri, M., Haardt, F. & Madau, P. The assembly and merging history of supermassive black holes in hierarchical models of galaxy formation. *Astrophys. J.* **582**, 559–573 (2003).
8. Wyithe, J. S. B. & Loeb, A. Self-regulated growth of supermassive black holes in galaxies as the origin of the optical and X-ray luminosity functions of quasars. *Astrophys. J.* **595**, 614–623 (2003).
9. Granato, G. L., De Zotti, G., Silva, L., Bressan, A. & Danese, L. A Physical model for the coevolution of QSOs and their spheroidal hosts. *Astrophys. J.* **600**, 580–594 (2004).
10. Mihos, J. C. & Hernquist, L. Gasdynamics and starbursts in major mergers. *Astrophys. J.* **464**, 641–663 (1996).
11. Soltan, A. Masses of quasars. *Mon. Not. R. Astron. Soc.* **200**, 115–122 (1982).
12. Yu, Q. & Tremaine, S. Observational constraints on growth of massive black holes. *Mon. Not. R. Astron. Soc.* **335**, 965–976 (2002).
13. Hernquist, L. Tidal triggering of starbursts and nuclear activity in galaxies. *Nature* **340**, 687–691 (1989).
14. Barnes, J. & Hernquist, L. Dynamics of interacting galaxies. *Annu. Rev. Astron. Astrophys.* **30**, 705–742 (1992).
15. Silk, J. & Rees, M. Quasars and galaxy formation. *Astron. Astrophys.* **334**, L1–L4 (1998).

16. Fabian, A. C. The obscured growth of massive black holes. *Mon. Not. R. Astron. Soc.* **308,** L39–L43 (1999).
17. King, A. Black holes, galaxy formation, and the M_{BH}–σ relation. *Astrophys. J.* **596,** L27–L29 (2003).
18. Chartas, G., Brandt, W. N. & Gallagher, S. C. XMM-Newton reveals the quasar outflow in PG 1115+080. *Astrophys. J.* **595,** 85–93 (2003).
19. Crenshaw, D. M., Kraemer, S. B. & George, I. M. Mass loss from the nuclei of active galaxies. *Annu. Rev. Astron. Astrophys.* **41,** 117–167 (2003).
20. Pounds, K. A. *et al.* A high-velocity ionized outflow and XUV photosphere in the narrow emission line quasar PG1211+143. *Mon. Not. R. Astron. Soc.* **345,** 705–713 (2003).
21. Springel, V., Di Matteo, T. & Hernquist, L. Modeling feedback from stars and black holes in galaxy mergers. *Mon. Not. R. Astron. Soc.* (submitted); Preprint astro-ph/0411108 at ⟨http://xxx.lanl.gov/⟩ (2004).
22. Bondi, H. On spherically symmetrical accretion. *Mon. Not. R. Astron. Soc.* **112,** 195–204 (1952).
23. Shakura, N. I. & Sunyaev, R. A. Black holes in binary systems. Observational appearance. *Astron. Astrophys.* **24,** 337–355 (1973).
24. Springel, V., Di Matteo, T. & Hernquist, L. Black holes in galaxy mergers: The formation of red elliptical galaxies. *Astrophys. J.* (submitted).
25. Springel, V. & Hernquist, L. Formation of a spiral galaxy in a major merger. *Astrophys. J.* (submitted).
26. Hasinger, G., Miyaji, T. & Schmidt, M. Luminosity dependent evolution of soft X-ray selected AGN. *Astron. Astrophys.* (submitted).
27. Barger, A. J. *et al.* The cosmic evolution of hard X-ray selected active galactic nuclei. *Astrophys. J.* (in the press).
28. Greene, J. E. & Ho, L. C. Active galactic nuclei with candidate intermediate-mass black holes. *Astrophys. J.* (in the press).
29. Springel, V. & Hernquist, L. Cosmological smoothed particle hydrodynamics simulations: a hybrid multiphase model for star formation. *Mon. Not. R. Astron. Soc.* **339,** 289–311 (2003).
30. Tremaine, S. *et al.* The slope of the black hole mass versus velocity dispersion correlation. *Astrophys. J.* **574,** 740–753 (2002).

....

Electronically soft phases in manganites

G. C. Milward, M. J. Calderón & P. B. Littlewood

Cavendish Laboratory, Cambridge University, Madingley Road, Cambridge CB3 0HE, UK

....

The phenomenon of colossal magnetoresistance in manganites[1] is generally agreed to be a result of competition between crystal phases with different electronic, magnetic and structural order; a competition which can be strong enough to cause phase separation between metallic ferromagnetic and insulating charge-modulated states[2–5]. Nevertheless, closer inspection of phase diagrams in many manganites reveals complex phases where the two order parameters of magnetism and charge modulation unexpectedly coexist[6,7]. Here we show that such experiments can be naturally explained within a phenomenological Ginzburg–Landau theory. In contrast to models where phase separation originates from disorder[8] or as a strain-induced kinetic phenomenon[9], we argue that magnetic and charge modulation coexist in new thermodynamic phases. This leads to a rich diagram of equilibrium phases, qualitatively similar to those seen experimentally. The success of this model argues for a fundamental reinterpretation of the nature of charge modulation in these materials, from a localized to a more extended 'charge-density wave' picture. The same symmetry considerations that favour textured coexistence of charge and magnetic order may apply to many electronic systems with competing phases. The resulting 'electronically soft' phases of matter with incommensurate, inhomogeneous and mixed order may be general phenomena in correlated systems.

The manganese perovskites ($RE^{3+}_{1-x}AE^{2+}_{x}MnO_3$, where RE is rare earth and AE is alkaline earth) provide a laboratory in which to study the interplay of a variety of magnetic, electronic and structural phases of matter in a strongly correlated electronic system. As in many strongly correlated electronic systems, the basic paradigm for manganite physics is the competition between the delocalizing effects of the electron kinetic energy and the localizing effects of the Coulomb repulsion, aided by coupling to lattice degrees of freedom. When the kinetic energy is dominant, one finds a metallic ground state with ferromagnetic alignment of the core moments. When the localizing effects are dominant, we see instead charge and orbitally ordered ground states with substantial local lattice distortions from the near-cubic symmetry of the metal, along with insulating behaviour and antiferromagnetism. We can tune between these two phases using any of several external parameters, especially chemical substitution, but also lattice strain and magnetic field. The competition between metal and insulator is evident in the phenomenon of bulk colossal magnetoresistance, in which a magnetic field tunes the conductivity of the material, and is even clearer in the strong tendency toward phase separation and inhomogeneity and regimes of percolative transport.

The origin of charge and orbital ordered phases is still the subject of debate. Charge modulation has been traditionally seen as the ordering of Mn^{4+} and Mn^{3+} ions[10]. More recently, the charge disproportionation of the Mn ions has been argued to be much smaller than one[11–13] but the idea of two kinds of cation-forming stripes still prevails and was used to interpret the experiments. In such a scenario, we would expect a density x of one kind of cation and $1-x$ of the other. The charge modulation would be given by the averaged wave vector $\mathbf{q} \approx (1-x)\mathbf{a}^\star$, where $\mathbf{a}^\star$ is the reciprocal lattice vector, aside from possible commensuration effects near special dopings ($x = 1/2, 2/3, 3/4$).

However, this picture is not compatible with the experimental findings on commensurate and incommensurate modulation that are summarized in Fig. 1a. At half-doping, commensurate modulation is expected and found at low temperatures, together with antiferromagnetism of the CE type[10]. Above the Néel temperature, though, the modulation is incommensurate[7,14]. When found to be charge-modulated, underdoped samples ($x < 0.5$) do not show the relation $\mathbf{q} \approx (1-x)\mathbf{a}^\star$; instead the modulation wave vector is always commensurate with $\mathbf{q} = 0.5\,\mathbf{a}^\star$ (refs 15–17) and independent of temperature. Finally, the overdoped samples ($x > 0.5$) show the expected incommensurate wave vector[18] below the Néel temperature, decreasing above it[19]. However, no sign of discommensurations, only a uniform incommensurate modulation, has been found in recent experiments on $La_{1-x}Ca_xMnO_3$ (ref. 20).

Another experimental conundrum is the coexistence of charge modulation and ferromagnetism despite their natural antipathy. For instance, at half-doping, the incommensurate modulation above the Néel temperature is accompanied by ferromagnetism[7]. A different electronic phase showing ferromagnetism and charge modulation has also been found at low temperature in $La_{0.5}Ca_{0.5}MnO_3$ (ref. 6). Slightly overdoped samples can also be ferromagnetic above the Néel temperature[21]. Another example of coexistence is given by the underdoped ($0.3 < x < 0.5$) $Pr_{1-x}Ca_xMnO_3$. The ground state is commensurate and charge-modulated[15,16] but the antiferromagnetism is canted[17,22], showing a ferromagnetic component coexisting with the commensurate charge modulation.

We might attempt to explain these phenomena in terms of microscopic theory, incorporating the many different couplings and microscopic degrees of freedom; this is a daunting task, however, that might not be illuminating, owing to its complexity. Here we propose a simple and more transparent phenomenological approach to this problem, using the Ginzburg–Landau theory[23–25].